Contrasting Effects of Hydrophobic and Hydrophilic Soft Surfaces on Ice Nucleation

Peicai Wu[a,b] and Quanzi Yuan *[a,b]

[a]State Key Laboratory of Nonlinear Mechanics, Institute of Mechanics, Chinese Academy of Sciences, Beijing 100190, China
[b]University of Chinese Academy of Sciences, Beijing 100049, People's Republic of China

Contents

*yuanquanzi@lnm.imech.ac.cn

1 Probabilistic Model of Nucleation Temperature Based on Classical Nucleation Theory

According to Classical Nucleation Theory (CNT), the nucleation rate $J(T)$, defined as the probability of nucleation per unit volume per unit time, is expressed as:

$$J(T) = J_0(T) \exp\left(-\frac{\Delta G(T)}{k_B T}\right)$$

where $J_0(T)$ is the kinetic pre-factor, k_B is the Boltzmann constant, T is the absolute temperature, and $\Delta G(T)$ is the free energy barrier for nucleation. The barrier is given by:

$$\Delta G(T) = \frac{16\pi\gamma^3 v_s^2 q}{3|\Delta\mu|^2}$$

Here, γ represents the ice-water interfacial free energy, $|\Delta\mu|$ is the chemical potential difference between ice and liquid water, v_s is the molecular volume of water in the ice phase, and q is a shape factor for the nucleus.

In our simulations, the system was cooled at a constant rate, described by $T(t) = T_0 - rt$, where the cooling rate is $r = 1$ K/ns and the initial temperature is $T_0 = 300$ K. Since the CNT model for ice nucleation is physically meaningful only below the melting point $T_m = 274.6$ K, we set the time origin ($t = 0$) at the moment when $T(t) = T_m$. The temperature evolution is therefore redefined as $T(t) = T_m - rt$ for $t \geq 0$. Consequently, the nucleation rate becomes a function of time, $J_t(t) = J(T_m - rt)$. This process can be modeled as a non-homogeneous Poisson process with an intensity $\lambda(t) = VJ_t(t)$, where V is the volume of the water.

The probability that no nucleation event has occurred by time t, known as the survival probability $S(t)$, is given by:

$$S(t) = P\{W_1 > t\} = 1 - P\{W_1 \leq t\} = \exp\left(-\int_0^t VJ_t(u)du\right)$$

where W_1 is the waiting time for the first nucleation event. The corresponding probability density function for the nucleation time is:

$$f(t) = VJ_t(t) \exp\left(-\int_0^t VJ_t(u)du\right)$$

The relationship between solid-liquid interfacial energy and temperature may be complex for different systems. However, for the ice-water interface, a widely used phenomenological relationship is given by:

$$\gamma(T) = \gamma_0 + a_\gamma(T_m - T)$$

For the mW water model, the parameters have been determined as $\gamma_0 = 35.028 \times 10^{-3}$ J/m^2 and $a_\gamma = -0.13648 \times 10^{-3}$ J/(K $\cdot$ m^2) [1,2].

The chemical potential difference at other temperatures can be derived using the Gibbs-Helmholtz equation:

$$\mu_l - \mu_s = -T \int_{T_m}^{T} \frac{h_l - h_s}{\theta^2}\, \mathrm{d}\theta$$

where h is the partial molar enthalpy. The difference in molar enthalpy, $h_l - h_s$, can be assumed to be independent of temperature and equal to the molar enthalpy of fusion $\Delta h_m = 1.26$ kcal/mol [3], the expression simplifies to:

$$\mu_l - \mu_s = \frac{\Delta h_m}{T_m}(T_m - T)$$

Substituting the expressions for $\gamma(T)$ and $\Delta\mu(T)$ into the equation for $\Delta G(T)$, we obtain:

$$\Delta G(T) = \frac{16\pi q v_s^2}{3} \frac{[\gamma_0 + a_\gamma(T_m - T)]^3 T_m^2}{\Delta h_m^2 (T_m - T)^2}$$

The kinetic pre-factor $J_0(T)$ is always assumed as a constant J_0 [4], the nucleation rate $J(T)$ is:

$$J(T) = J_0 \exp\left\{-\frac{16\pi q v_s^2}{3k_B T} \frac{[\gamma_0 + a_\gamma(T_m - T)]^3 T_m^2}{\Delta h_m^2 (T_m - T)^2}\right\}$$

Using the relation $T = T_m - rt$, the time-dependent nucleation rate $J_t(t)$ becomes:

$$J_t(t) = J_0 \exp\left\{-\frac{16\pi q v_s^2 T_m^2}{3k_B \Delta h_m^2} \frac{[\gamma_0 + a_\gamma rt]^3}{(T_m - rt)(rt)^2}\right\}$$

Nondimensionalization

To simplify the analysis, we introduce a dimensionless time $\tau = \frac{rt}{T_m}$. The nucleation rate as a function of τ is then:

$$J_\tau(\tau) = J_t(t(\tau)) = J_0 \exp\left[-\frac{16\pi q v_s^2 \gamma_0^3}{3k_B T_m \Delta h_m^2} \frac{(1+\frac{a_\gamma T_m}{\gamma_0}\tau)^3}{(1-\tau)\tau^2}\right]$$

The probability density function of the nucleation time, $f(t)$, can be transformed into a probability density function of the dimensionless time, $\hat{f}(\tau)$:

$$\begin{aligned}\hat{f}(\tau) &= \frac{T_m}{r} f(t) \\ &= \frac{VT_m}{r} J_\tau(\tau) \exp\left(-\int_0^\tau \frac{VT_m}{r} J_\tau(v) dv\right) \\ &= \hat{\lambda}(\tau) \exp\left(-\int_0^\tau \hat{\lambda}(v) dv\right)\end{aligned}$$

The survival curve in terms of dimensionless time is:

$$\hat{S}(\tau) = \exp\left(-\int_0^\tau \hat{\lambda}(v) dv\right)$$

where $\hat{\lambda}(\tau)$ is the dimensionless nucleation rate:

$$\begin{aligned}\hat{\lambda}(\tau) &= \frac{VT_m}{r} J_\tau(\tau) \\ &= \frac{VT_m J_0}{r} \exp\left\{-\frac{16\pi q v_s^2 \gamma_0^3}{3k_B T_m \Delta h_m^2} \frac{\left(1+\frac{a_\gamma T_m}{\gamma_0}\tau\right)^3}{(1-\tau)\tau^2}\right\} \\ &= \exp(A - bg(\tau))\end{aligned}$$

Here, A and b are dimensionless parameters:

$$A = \ln \frac{VT_m J_0}{r}, \quad b = \frac{16\pi q v_s^2 \gamma_0^3}{3k_B T_m \Delta h_m^2}$$

These parameters represent the kinetic factor and the nucleation barrier factor, respectively. The function $g(\tau)$ is defined as:

$$g(\tau) = \frac{\left(1+\frac{a_\gamma T_m}{\gamma_0}\tau\right)^3}{(1-\tau)\tau^2} = \frac{(1-1.07\tau)^3}{(1-\tau)\tau^2}$$

In some simplified models, a_γ is assumed to be zero. We have verified that the main conclusions of our study are insensitive to the precise value of a_γ.

Maximum Likelihood Estimation (MLE)

The observed nucleation temperatures T_i from simulations were converted into dimensionless nucleation time τ_i. The probability density function for these events is $\hat{f}(\tau)$. We employed MLE to find the optimal parameters A and b that maximize the likelihood function $L(\tau_i; A, b)$:

$$L(\tau_i; A, b) = \prod_{i=1}^{N} \hat{f}(\tau_i)$$

where N is the number of independent simulations. This is equivalent to maximizing the log-likelihood function:

$$\ln(L(\tau_i; A, b)) = \sum_{i=1}^{N} \ln(\hat{f}(\tau_i))$$

This optimization problem was solved using the Nelder-Mead algorithm implemented in a Python script. The uncertainties in the estimated parameters (A, b) were assessed using a bootstrap method with 2000 resamples.

Model Refinement with Microscopic Kinetics

We refined the model by incorporating a temperature-dependent kinetic pre-factor $J_0(T)$. The time-dependent nucleation rate is now:

$$J_t(t) = J_0(T(t)) \exp\left\{ -\frac{16\pi q v_s^2 T_m^2}{3k_B \Delta h_m^2} \frac{[\gamma_0 + a_\gamma rt]^3}{(T_m - rt)(rt)^2} \right\}$$

where the pre-factor is given by [5, 6]:

$$J_0(T) = \frac{N_l k_B T}{h} \exp\left(-\frac{\Delta g}{k_B T} \right)$$

Here, N_l is the number density of water molecules in the liquid phase, and h is the Planck constant.

The functional form of the activation energy for diffusion across the interface, Δg, is not universally agreed upon. To account for the slowing down of interfacial water dynamics at lower temperatures, we adopted a phenomenological model assuming $\Delta g \propto 1/T$. This leads to:

$$\Delta g = \frac{D}{1-\tau} k_B T_m$$

where D is a dimensionless parameter. Substituting $T = T_m(1-\tau)$, the pre-factor becomes:

$$J_0(T(\tau)) = \frac{N_l k_B T_m}{h} (1-\tau) \exp\left(-\frac{D}{(1-\tau)^2} \right)$$

The dimensionless nucleation rate $\hat{\lambda}(\tau)$ is then modified to:

$$\begin{aligned}
\hat{\lambda}(\tau) &= \frac{VT_m}{r} J_\tau(\tau) \\
&= \frac{VT_m}{r} J_0(T(\tau)) \exp(-bg(\tau)) \\
&= \frac{VT_m}{r} \frac{N_l k_B T_m}{h} (1-\tau) \exp\left[-\frac{D}{(1-\tau)^2} - bg(\tau) \right] \\
&= (1-\tau) \exp\left[A' - \frac{D}{(1-\tau)^2} - bg(\tau) \right]
\end{aligned}$$

Based on parameters from Ref. [6], we can estimate the order of magnitude of A':

$$A' = \ln\left(\frac{VT_m}{r} \frac{N_l k_B T_m}{h} \right) \approx \ln(1.6 \times 10^{10})$$

For numerical consistency, we introduce a scaling factor a' such that:

$$A' = a' \ln(1.6 \times 10^{10})$$

The final expression for the dimensionless rate is:

$$\hat{\lambda}(\tau) = (1-\tau) \exp\left[a' \ln(1.6 \times 10^{10}) - \frac{D}{(1-\tau)^2} - bg(\tau) \right]$$

The probability distribution function remains $\hat{f}(\tau) = \hat{\lambda}(\tau) \exp\left(-\int_0^\tau \hat{\lambda}(v) dv \right)$. We performed MLE for the parameters (a', D, b) using a simulated annealing algorithm. The estimated parameters are summarized in Table S1. The refined survival curve is presented as Figure 7 in the main text.

Table S1: Parameters from the refined CNT model.

Surface	b	D	a'
Hydrophobic	1.42 ± 0.35	46.61 ± 14.94	4.20 ± 1.22
Hydrophilic	4.15 ± 1.32	43.20 ± 19.19	4.86 ± 1.91

Normalization of the Survival Curve

$$\hat{f}(\tau) = \hat{\lambda}(\tau) \exp\left(-\int_0^\tau \hat{\lambda}(v)dv\right)$$

The cumulative distribution function is:

$$\begin{aligned} P\{W_1 \leq \tau\} &= \int_0^\tau \hat{f}(v)dv \\ &= 1 - \exp\left(-\int_0^\tau \hat{\lambda}(v)dv\right) \\ &= 1 - \hat{S}(\tau) \end{aligned}$$

Thus, the survival curve is $\hat{S}(\tau) = 1 - \int_0^\tau \hat{f}(v)dv$. As $\tau \to \infty$, $\hat{S}(\tau)$ naturally approaches 0 because $\hat{\lambda}(\tau)$ is always positive, ensuring that $\hat{f}(\tau)$ is normalized over $[0, \infty)$. However, in a constant cooling rate process, the dimensionless time τ is practically bounded within $[0, 1]$. Therefore, we normalize the distributions over this interval. The normalization constant is:

$$I = \int_0^1 \hat{f}(\tau)d\tau = 1 - \hat{S}(1)$$

The normalized function is:

$$\hat{f}_{\text{norm}}(\tau) = \frac{\hat{f}(\tau)}{1 - \hat{S}(1)}$$

And the normalized survival curve is:

$$\begin{aligned} \hat{S}_{\text{norm}}(\tau) &= 1 - \frac{\int_0^\tau \hat{f}(v)dv}{I} \\ &= 1 - \frac{1 - \hat{S}(\tau)}{1 - \hat{S}(1)} \\ &= \frac{\hat{S}(\tau) - \hat{S}(1)}{1 - \hat{S}(1)} \end{aligned}$$

2 Calculation of Interfacial Water Residence Time

Density Profile and Definition of the Interfacial Water Region

The surface of the PVA aggregate is flexible, making a precise, atomistic definition of the surface challenging. To overcome this, we first identified the first layer of water molecules covering the surface and calculated the mean z-coordinate of these molecules, denoted as z_0. Subsequently, we computed the water density profile $\rho(z)$ along the z-axis for the equilibrated liquid phase at different temperatures, using z_0 as the reference origin $z = 0$. The density profile is shown in Figure S1.

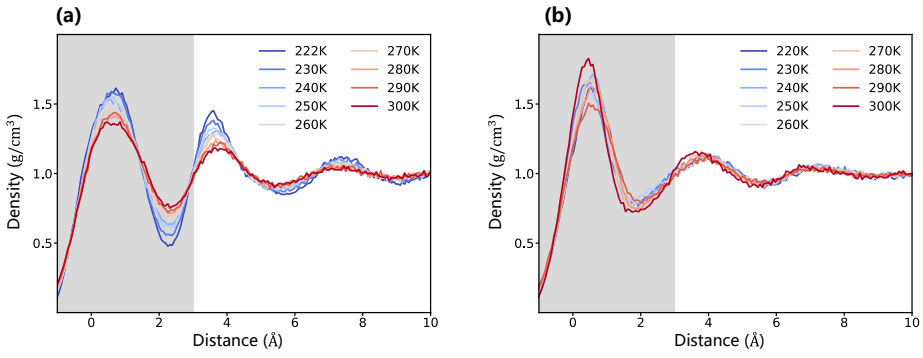

Figure S1: Water density profile $\rho(z)$ as a function of distance from the reference surface position z_0 for (a) the hydrophobic surface and (b) the hydrophilic surface. The shaded area indicates the defined interfacial region.

Comparing the two surfaces, the most notable difference is the first density peak. The hydrophilic surface (Figure S1b) exhibits a sharper and narrower primary peak, indicating that water molecules are highly localized and pinned by the surface hydroxyls. In contrast, the broader peak on the hydrophobic surface (Figure S1a) reflects a weaker confinement and greater structural flexibility of interfacial water.

The region $z < z_0 + 0.3$ nm (shaded in gray) encompasses the first peak and the first minimum of the water density profile. We therefore define this slab as the interfacial water region. All subsequent analyses of interfacial water properties are based on this definition.

Radial Distribution Function Analysis

To further quantify the local, short-range intermolecular interactions that determine the surface hydrophobicity, we calculated the radial distribution functions (RDFs) between the surface interacting sites and the interfacial water molecules (Figure S2).

The analysis focuses on the position of the first coordination shell, which defines the physical characteristics of the surface-water interface. For the hydrophobic surface, the RDF was calculated between the carbon backbone and water (Figure S2a). The first interaction peak emerges at a relatively large distance of $\sim$ 3.8 Å. This is the characteristic distance for van der Waals interactions, confirming that water molecules do not form hydrogen bonds with the carbon backbone. In contrast, for the hydrophilic surface, the RDF between the surface hydroxyl groups and water (Figure S2b) displays a highly intense and sharp first peak at $\sim$ 2.8 Å. This specific distance is characteristic of strong hydrogen bonds formed between surface hydroxyl groups and water. This strong interaction directly validates the pronounced pinning effect and the highly localized density peak observed in Figure S1b.

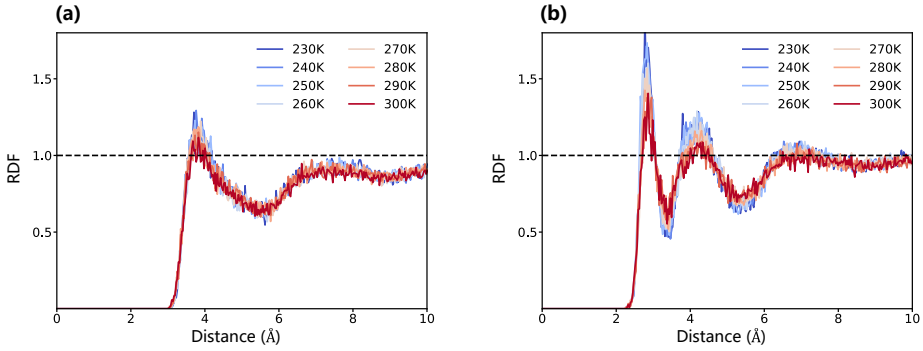

Figure S2: Radial distribution functions (RDFs) between the surface interacting sites and water molecules at various temperatures for (a) the hydrophobic surface and (b) the hydrophilic surface.

Interfacial Water Indicator Function and Correlation Analysis

To quantify water residence time, we defined an indicator function $h_i(t)$ for each water molecule i that ever entered the interfacial region. For a given molecule i, $h_i(t_j) = 1$ if it is located within the interfacial region at time t_j, and $h_i(t_j) = 0$ otherwise. Following established methods for calculating hydrogen bond lifetimes [7, 8], we computed the normalized time autocorrelation function of this indicator function, $c(t) = \frac{\langle h(t)h(0)\rangle}{\langle h(0)h(0)\rangle}$. The function $c(t)$ represents the probability that a water molecule being in the interfacial region at time $t = 0$ is still present in the same region at time t.

Due to the flexible nature of the surface and the presence of adsorption sites, $c(t)$ may not decay to zero within the simulation timescale but exhibits a continuous decay. We fitted the $c(t)$ to a stretched exponential function: $c'(t) = a + (1 - a)\exp[-(t/\tau_r)^\beta]$, where τ_r is a characteristic relaxation time. We define the mean residence time, $t_{1/2}$, as the time at which the probability has decayed to half of its initial mobile fraction, i.e., $\exp[-(t_{1/2}/\tau_r)^\beta] = 1/2$, yielding $t_{1/2} = \tau_r(\ln 2)^{1/\beta}$. Figure S3 shows the fits of the function, and the resulting mean residence times are presented in the main text.

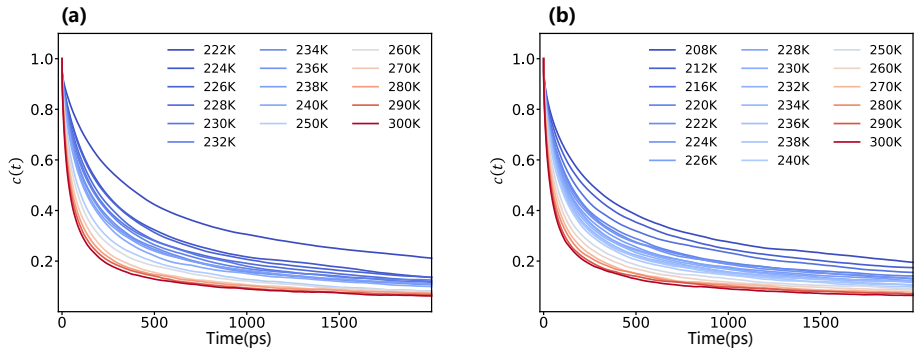

Figure S3: Autocorrelation function $c(t)$ for interfacial water molecules at different temperatures for (a) the hydrophobic surface and (b) the hydrophilic surface. Solid lines represent fits to the stretched exponential function.

3 Effect of Cooling Rate on Nucleation Temperature

To explicitly demonstrate that our conclusions are robust, we performed additional sets of independent MD simulations at slower cooling rates of 0.5 K/ns and 0.2 K/ns. All other simulation protocols remained identical to those described in the Methods section of the main text.

As shown in Figure S4, the nucleation temperatures T_n for both systems shift to higher values as the cooling rate decreases. This behavior is consistent with the theoretical expectation discussed in the main text. More importantly, the results confirm that the pronounced temperature difference ($\sim$ 15 K) between the hydrophobic and hydrophilic surfaces is consistently maintained across all tested cooling rates.

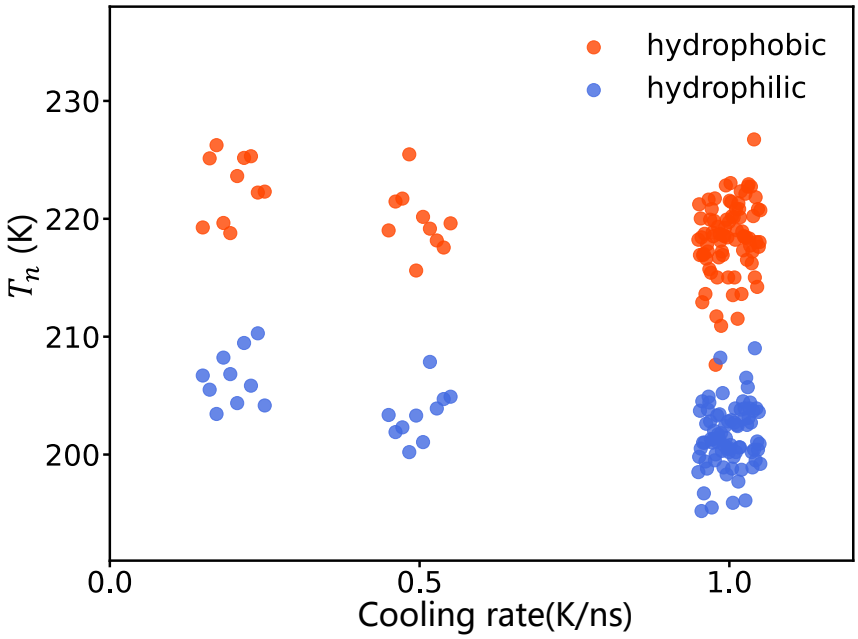

Figure S4: Distribution of ice nucleation temperatures T_n at varying cooling rates (0.2, 0.5, and 1.0 K/ns). Each point represents an independent simulation run. While the average T_n increases with a slower cooling rate, the substantial difference in nucleation activity between the hydrophobic and hydrophilic surfaces remains robust.

4 Functional Form of the mW Water Model Potential

As described in the main text, the coarse-grained mW water model [3] and the interactions involving the hydroxyl groups of PVA do not employ explicit electrostatic charges. Instead, they interact via the Stillinger-Weber (SW) potential [9], which implicitly captures the hydrogen-bonding interactions. The total potential energy of the system is expressed as the sum of two-body and three-body interactions:

$$U = \sum_i \sum_{j>i} \varphi_2(r_{ij}) + \sum_i \sum_{j\neq i} \sum_{k>j} \varphi_3(r_{ij}, r_{ik}, \theta_{ijk}).$$

Here, φ_2 is the two-body term that accounts for short-range interactions, depending only on the distance r_{ij} between particles i and j:

$$\varphi_2(r_{ij}) = A\varepsilon \left[B \left(\frac{\sigma}{r_{ij}} \right)^p - \left(\frac{\sigma}{r_{ij}} \right)^q \right] \exp\left(\frac{\sigma}{r_{ij} - a\sigma} \right).$$

The three-body term φ_3 introduces an energetic penalty for non-tetrahedral configurations, which efficiently captures the directionality of hydrogen bonds. It depends on the distances r_{ij} and r_{ik}, and the angle θ_{ijk} formed by particles i, j, and k:

$$\varphi_3(r_{ij}, r_{ik}, \theta_{ijk}) = \lambda\varepsilon[\cos\theta_{ijk} - \cos\theta_0]^2 \exp\left(\frac{\gamma\sigma}{r_{ij} - a\sigma} \right) \exp\left(\frac{\gamma\sigma}{r_{ik} - a\sigma} \right),$$

where the ideal tetrahedral angle is set by $\cos\theta_0 = -1/3$, and the parameters $(A, B, p, q, a, \lambda, \gamma, \varepsilon, \sigma)$ for water-water and water-hydroxyl interactions are identical and were adopted from the original mW model parametrization [3]. The interactions between the PVA hydrocarbon backbone and water are modeled solely by standard Lennard-Jones potentials.

References

[1] Jorge R. Espinosa, Carlos Vega, Chantal Valeriani, and Eduardo Sanz. Seeding approach to crystal nucleation. *J. Chem. Phys.*, 144(3):034501, 2016.

[2] J. R. Espinosa, C. Navarro, E. Sanz, C. Valeriani, and C. Vega. On the time required to freeze water. *J. Chem. Phys.*, 145(21):211922, 2016.

[3] Valeria Molinero and Emily B. Moore. Water Modeled As an Intermediate Element between Carbon and Silicon. *J. Phys. Chem. B*, 113(13):4008–4016, 2009.

[4] Raffaela Cabriolu and Tianshu Li. Ice nucleation on carbon surface supports the classical theory for heterogeneous nucleation. *Phys. Rev. E*, 91(5):052402, 2015.

[5] Thomas Koop and Benjamin J. Murray. A physically constrained classical description of the homogeneous nucleation of ice in water. *J. Chem. Phys.*, 145(21):211915, 2016.

[6] Luisa Ickes, André Welti, Corinna Hoose, and Ulrike Lohmann. Classical nucleation theory of homogeneous freezing of water: thermodynamic and kinetic parameters. *Phys. Chem. Chem. Phys.*, 17(8):5514–5537, 2015.

[7] Meijia Qiu, Peng Sun, Kai Han, Zhenjiang Pang, Jun Du, Jinliang Li, Jian Chen, Zhong Lin Wang, and Wenjie Mai. Tailoring water structure with high-tetrahedral-entropy for antifreezing electrolytes and energy storage at -80 °C. *Nat. Commun.*, 14(1):601, 2023.

[8] Raviteja Kurapati and Upendra Natarajan. Factors responsible for the aggregation of poly(vinyl alcohol) in aqueous solution as revealed by molecular dynamics simulations. *Ind. Eng. Chem. Res.*, 59(37):16099–16111, 2020.

[9] Frank H Stillinger and Thomas A Weber. Computer simulation of local order in condensed phases of silicon. *Physical review B*, 31(8):5262, 1985.